Neuron
NeuroResource

In Vivo Expression of a Light-Activatable Potassium Channel Using Unnatural Amino Acids

Ji-Yong Kang,[1] Daichi Kawaguchi,[2] Irene Coin,[1] Zheng Xiang,[1] Dennis D.M. O'Leary,[2] Paul A. Slesinger,[3,4] and Lei Wang[1,*]
[1]The Jack H. Skirball Center for Chemical Biology and Proteomics
[2]Molecular Neurobiology Laboratory
[3]Peptide Biology Laboratory
The Salk Institute for Biological Studies, La Jolla, CA 92037, USA
[4]Department of Neuroscience, Icahn School of Medicine at Mount Sinai, New York, NY 10029, USA
*Correspondence: lwang@salk.edu
http://dx.doi.org/10.1016/j.neuron.2013.08.016

SUMMARY

Optical control of protein function provides excellent spatial-temporal resolution for studying proteins in situ. Although light-sensitive exogenous proteins and ligands have been used to manipulate neuronal activity, a method for optical control of neuronal proteins using unnatural amino acids (Uaa) in vivo is lacking. Here, we describe the genetic incorporation of a photoreactive Uaa into the pore of an inwardly rectifying potassium channel Kir2.1. The Uaa occluded the pore, rendering the channel nonconducting, and, on brief light illumination, was released to permit outward K^+ current. Expression of this photoinducible inwardly rectifying potassium (PIRK) channel in rat hippocampal neurons created a light-activatable PIRK switch for suppressing neuronal firing. We also expanded the genetic code of mammals to express PIRK channels in embryonic mouse neocortex in vivo and demonstrated a light-activated PIRK current in cortical neurons. These principles could be generally expanded to other proteins expressed in the brain to enable optical regulation.

INTRODUCTION

The ability to control protein function with light provides excellent temporal and spatial resolution for precise investigation in vitro and in vivo and, thus, is having significant impact on neuroscience. For example, naturally light-sensitive opsin channels and pumps have been exploited to excite or inhibit neurons, enabling specific modulation of selected cells and circuits in diverse model organisms (Bernstein and Boyden, 2011; Fenno et al., 2011; Yizhar et al., 2011). However, since this approach relies on the ectopic expression of an exogenous or chimera protein requiring retinal as the chromophore, it cannot be applied to control a particular endogenous protein. Another elegant method engineers light responsiveness into endogenous receptors and channels by chemically tethering a photoswitchable azobenzene-coupled ligand (Szobota and Isacoff, 2010). The ligand is presented or withdrawn from the binding site of the protein through the photoisomerization of the azobenzene moiety. This approach cannot address proteins that are expressed but failed to conjugate with the azobenzene-coupled ligand, and ligand tethering has been limited to the extracellular side of membrane proteins, excluding the intracellular side and intracellular proteins.

Photoresponsive unnatural amino acids (Uaas) provide another flexible avenue for optical control of protein activities. Microinjection of tRNAs chemically acylated with Uaas allows the incorporation of photocaging groups into receptors and ion channels in *Xenopus oocytes*, which have revealed novel insights on their structure and function (England et al., 1997; Miller et al., 1998; Philipson et al., 2001). The requirement of microinjection has mainly limited this approach to large oocytes. Genetically encoding Uaas with orthogonal tRNA/synthetase pairs enables the Uaa to be incorporated into proteins with high protein yields in mammalian cells and organisms (Liu and Schultz, 2010; Wang et al., 2001, 2006, 2009), providing potential for studying proteins with Uaas directly in primary neurons and mouse models (Shen et al., 2011; Wang et al., 2007). A challenge in the neuroscience field, however, has been the application of Uaa technology in mammalian neurons in vitro and, ultimately, in the mouse brain in vivo.

Here, we demonstrate the optical control of a neuronal protein in vitro and in vivo using a genetically encoded photoreactive Uaa. Kir2.1 is a strong inwardly rectifying potassium channel that is crucial in regulating neuronal excitability, action potential cessation, hormone secretion, heart rate, and salt balance (Bichet et al., 2003). We incorporated 4,5-dimethoxy-2-nitrobenzyl-cysteine (Cmn) into the pore of Kir2.1, generating a *p*hotoactivatable *i*nwardly *r*ectifying potassium (which we refer to as PIRK) channel. Light activation of PIRK channels expressed in rat hippocampal neurons suppressed neuronal firing. In addition, we expressed PIRK channels in embryonic mouse neocortex, measured light-activated PIRK current in cortical neurons, and showed the potential for its use in other brain regions such as diencephalon, demonstrating the successful implementation of the Uaa technology in vivo in the mammalian brain. Genetically

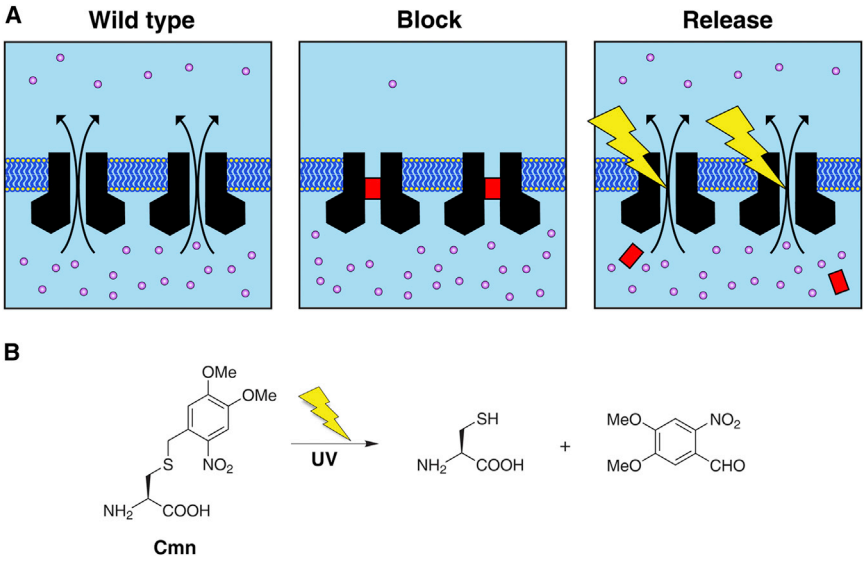

Figure 1. PIRK Channel using Genetic Incorporation of Photocaged Uaas

(A) A model illustrating photoactivation of PIRK channels expressed on the plasma membrane. Left: wild-type Kir2.1 channels (black) conduct K^+ (in purple) current in physiological conditions. Middle: incorporating the Uaa Cmn (in red) in the pore of Kir2.1 channels renders the channel nonconducting (PIRK channels). Right: UV light exposure irreversibly removes the dimethoxynitrobenzyl group to allow permeation through the Kir2.1 channel, restoring outward K^+ (in purple) current and reducing membrane excitability.

(B) Chemical pathway for photolysis of Cmn. UV light cleaves the S–C bond, releasing the dimethoxynitrobenzyl group from Cys. Cys would remain on the protein.

encoding Uaas has no limitations on protein type and location (Wang and Schultz, 2004), and photocaging is compatible with modulating various proteins (Adams and Tsien, 1993; Fehrentz et al., 2011). We therefore expect that our method can be generally applied to other brain proteins, enabling optical investigation of a range of channels, receptors, and signaling proteins in the brain.

RESULTS

Construction of a PIRK Channel with Genetically Encoded Photocaged Uaas

Potassium ions flow through the central pore of Kir2.1 channels (Ishii et al., 1994; Kubo et al., 1993). We reasoned that incorporation of a Uaa with a bulky side chain might occlude the channel pore and restrict current flow. Photolysis of the Uaa would enable release of the bulky side chain moiety and restore current flow through the channel, thus creating a PIRK channel (Figure 1A). Ideally, a natural amino acid residue can be regenerated from the Uaa after photolysis, minimizing potential perturbation to protein structure and function. Cmn is a perfect Uaa for constructing a PIRK channel. The dimethoxynitrobenzyl group of Cmn is readily hydrolyzed by UV light, releasing the cage group and becoming Cys (Figure 1B; Figure S2A available online) (Rhee et al., 2008). Compared to the conventional photocaging *o*-nitrobenzyl group, the dimethoxynitrobenzyl group is bulkier and has a higher quantum yield to facilitate photolysis. Previously, 4,5-dimethoxy-2-nitrobenzyl serine was incorporated into the transcription factor Pho4 in *Saccharomyces cerevisiae* to control phosphorylation with light (Lemke et al., 2007). Based on the similar structure and characteristics between serine and cysteine, we hypothesized that the orthogonal $tRNA^{Leu}_{CUA}$ /synthetase pair evolved in yeast to incorporate 4,5-dimethoxy-2-nitrobenzyl serine might also selectively incorporate Cmn. Indeed, Cmn was efficiently incorporated into proteins in mammalian cells by this pair, which we refer to as $tRNA^{Leu}_{CUA}$ /CmnRS for clarity. Cmn was chosen for incorporation because multiple sites of Kir2.1 are found permissive for Cys mutation, and the sulfhydryl group of Cys also provides a chemically reactive functionality for possible secondary modifications if required.

To achieve photoactivation of Kir2.1 using Cmn, we considered the following criteria for identifying a target site for incorporation into the channel protein: (1) the site should reside in the channel pore where the side chain of Cmn would face the pore lumen and be easily removed following photocleavage; (2) the pore should be large enough to accommodate four Cmn molecules in a Kir2.1 tetramer without disrupting protein folding but become small enough after Cmn incorporation to efficiently inhibit ion current flow; and (3) a site where a Cys mutation would not likely interfere with Kir2.1 function.

Using published data on Kir2.1 pore topology and function (Kubo et al., 1993; Lu et al., 1999a; Minor et al., 1999; Tao et al., 2009) and the crystal structure of chicken Kir2.2 (Tao et al., 2009), we identified 15 amino acids in the pore of rat Kir2.1 (which has 76% sequence homology with chicken Kir2.2) with side chains that face the pore lumen (K117, V118, A131, T142, I143, C149, V150, D152, S165, C169, D172, I176, M180, A184, and E224). Previous studies indicated that Cys substitution at T142, I143, D172, I176, A184, or E224 did not interfere with Kir2.1 function (Dart et al., 1998; Kubo et al., 1998; Lu et al., 1999a, 1999b; Minor et al., 1999; Xiao et al., 2003). Therefore, these six amino acids plus C149 and C169 were selected for Cmn incorporation (Figure 2A; Figures S1A and S1B).

The codon for these candidate sites was first mutated to the amber stop codon TAG to generate eight different mutant *Kir2.1* (*Kir2.1*$_{TAG}$) genes. The *Kir2.1*$_{TAG}$ cDNA was individually coexpressed with the orthogonal $tRNA^{Leu}_{CUA}$/CmnRS pair in human embryonic kidney 293T (HEK293T) cells. On exogenous addition of the Uaa Cmn to growth media, the CmnRS aminoacylates Cmn on to the $tRNA^{Leu}_{CUA}$, which, in turn, recognizes the amber stop codon (UAG) in *Kir2.1* mRNA and incorporates Cmn into Kir2.1 protein during translation (Wang et al., 2001; Wang and Schultz, 2004).

Each candidate site was initially tested whether it was permissive for UAG suppression by the orthogonal $tRNA^{Leu}_{CUA}$/leucyl-tRNA synthetase (LeuRS) pair, which incorporates the natural

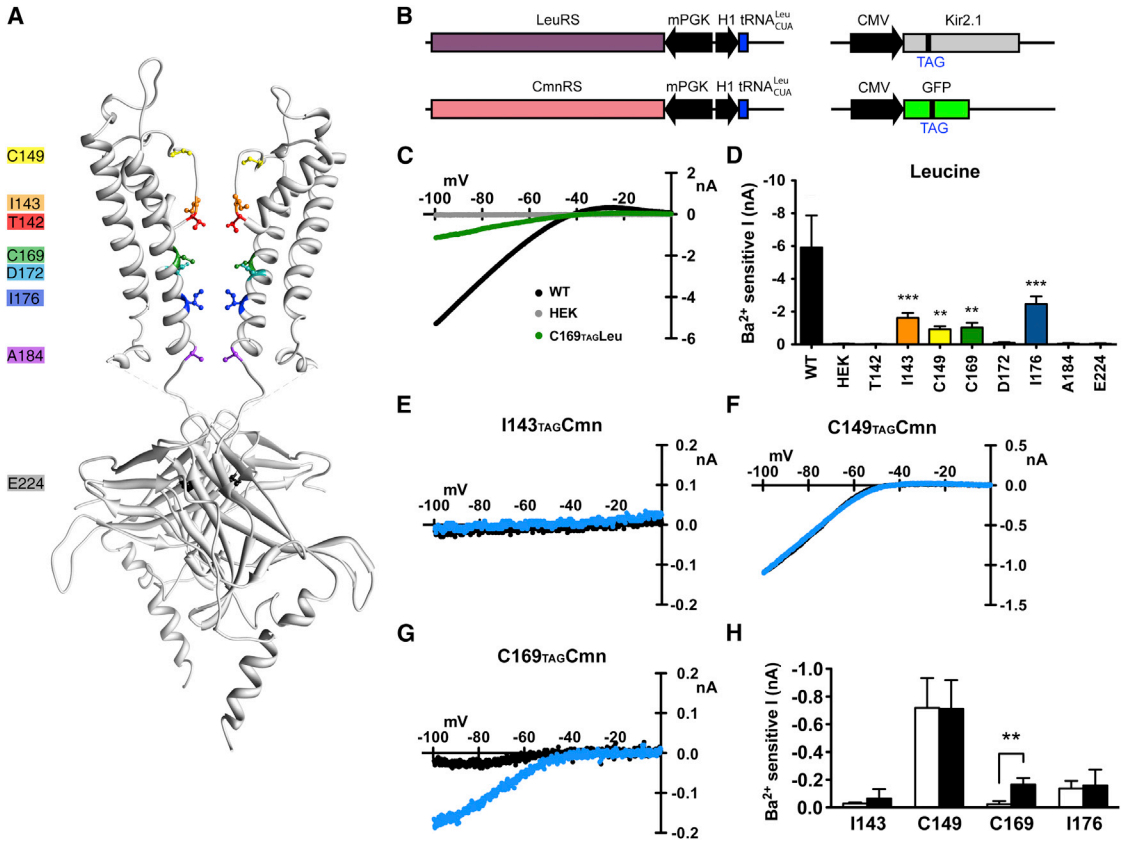

Figure 2. Identification of a Critical Site in Kir2.1 for Cmn Incorporation that Enables Photoactivation

(A) Side view of the crystal structure of chicken Kir2.2 channel (Protein Data Bank ID: 3JYC) showing positions of candidate sites for incorporating Cmn. Two of four subunits are shown for clarity. Eight residues that potentially contribute to ion permeation are highlighted: T142 (red), I143 (orange), C149 (yellow), C169 (green), D172 (light blue), I176 (navy), A184 (purple), and E224 (black). Molecular drawings were prepared using UCSF Chimera 1.6.2.

(B) Design of expression plasmids for Uaa mutagenesis. A plasmid for Leu incorporation, the amber suppressing orthogonal $tRNA^{Leu}_{CUA}$ driven by the H1 promoter and the aminoacyl-tRNA synthetase *LeuRS* driven by the mPGK promoter. A plasmid for Cmn incorporation, $tRNA^{Leu}_{CUA}$ driven by the H1 promoter and the aminoacyl-tRNA synthetase *CmnRS* driven by the mPGK promoter. A plasmid encoding *Kir2.1* with the amber stop codon TAG and driven by the CMV promoter. A plasmid for the GFP reporter gene (*GFP_Y182$_{TAG}$*) driven by the CMV promoter.

(C) The current-voltage (I-V) plot of currents recorded from HEK293T cells expressing wild-type *Kir2.1* (WT; black), expressing *Kir2.1_C169$_{TAG}$Leu* with $tRNA^{Leu}_{CUA}$ */LeuRS* (C169$_{TAG}$Leu; green), or untransfected (HEK; gray).

(D) Mean Ba^{2+}-sensitive currents (I_{Kir}) for eight amber stop codon (TAG) mutations. Four sites in Kir2.1 were permissive for UAG suppression with Leu (I143, C149, C169, and I176). Ba^{2+}-sensitive currents at −100 mV (mean ± SEM) were as follows: WT Kir2.1 (−5.92 ± 1.95 nA, n = 4), untransfected HEK293T cells (−0.05 ± 0.02 nA, n = 9), T142$_{TAG}$Leu (−0.03 ± 0.02 nA, n = 5), I143$_{TAG}$Leu (−1.62 ± 0.30 nA, n = 5), C149$_{TAG}$Leu (−0.92 ± 0.20 nA, n = 6), C169$_{TAG}$Leu (−1.03 ± 0.29 nA, n = 5), D172$_{TAG}$Leu (−0.10 ± 0.05 nA, n = 5), I176$_{TAG}$Leu (−2.46 ± 0.47 nA, n = 4), A184$_{TAG}$Leu (−0.05 ± 0.04 nA, n = 4), and E224$_{TAG}$Leu (−0.04 ± 0.04 nA, n = 4). **p < 0.01 and ***p < 0.001, one-way ANOVA. WT Kir2.1 was excluded from statistical analysis.

(E–G) Examples of I-V plots for three different Kir2.1 channels with Cmn incorporation before (black) and after (blue) UV illumination (385 nm, 40 mW/cm^2, 1 s). Cmn was incorporated at the indicated sites by the orthogonal $tRNA^{Leu}_{CUA}$ /CmnRS.

(H) Ba^{2+}-sensitive current (I_{Kir}) measured at −100 mV before (open column) and after (filled column) light exposure from HEK293T cells expressing different Kir2.1 channels with Cmn incorporation. One second of 385 nm light pulse at 40 mW/cm^2 was applied. Only incorporation of Cmn at the C169 site led to a channel where light exposure increased the current above background levels. Mean Ba^{2+}-sensitive currents ± SEM were as follows: I143$_{TAG}$Cmn (before: −0.03 ± 0.01 nA; after: −0.07 ± 0.07 nA, n = 4), C149$_{TAG}$Cmn (before: −0.72 ± 0.21 nA; after: −0.71 ± 0.21 nA, n = 3), C169$_{TAG}$Cmn (before: −0.02 ± 0.02 nA; after: −0.17 ± 0.05 nA, n = 7), and I176$_{TAG}$Cmn (before: −0.14 ± 0.05 nA, after: −0.16 ± 0.11 nA, n = 8). **p < 0.01, paired t test.

See also Figure S1.

amino acid leucine (Leu). Each *Kir2.1$_{TAG}$* gene was transfected into HEK293T cells along with the *$tRNA^{Leu}_{CUA}$/LeuRS* (Figure 2B). The gene for green fluorescent protein (GFP) engineered with an amber stop codon at Tyr182 (*GFP_Y182$_{TAG}$*) was cotransfected (Wang et al., 2007). GFP fluorescence would indicate the successful suppression of the UAG stop codon by the orthogonal tRNA/synthetase. The function of individual Kir2.1$_{TAG}$ channels was then determined by whole-cell patch-clamp recordings from GFP-positive cells. For example, a green-positive HEK293T cell transfected with *Kir2.1_C169$_{TAG}$* and the *$tRNA^{Leu}_{CUA}$/LeuRS* produced a basally active inwardly rectifying current that was inhibited by extracellular Ba^{2+} (I_{Kir}), similar to wild-type Kir2.1 channels (Figure 2C). Of the eight candidate sites, I_{Kir} currents measured at −100 mV from HEK293T cells

expressing *Kir2.1_I143$_{TAG}$*, *Kir2.1_C149$_{TAG}$*, *Kir2.1_C169$_{TAG}$*, or *Kir2.1_I176$_{TAG}$* were significantly larger than those from untransfected cells (Figure 2D), indicating successful suppression and incorporation of Leu.

If a functional Kir2.1 channel could be generated through Leu incorporation at the TAG site, then it seemed likely that the same site would be compatible for the larger Uaa Cmn. We therefore tested *Kir2.1_I143$_{TAG}$*, *Kir2.1_C149$_{TAG}$*, *Kir2.1_C169$_{TAG}$*, and *Kir2.1_I176$_{TAG}$* for functional incorporation of Cmn (Figures 2E–2H; Figure S1C). HEK293T cells were transfected with cDNAs for the Kir2.1$_{TAG}$ channel, tRNA$^{Leu}_{CUA}$/CmnRS and the GFP_Y182$_{TAG}$ reporter (Figure 2B), and incubated in Cmn (1 mM) for 12–24 hr. Functional incorporation of Cmn was expected to lead to either a basally active I_{Kir} or an I_{Kir} that is revealed upon brief (1 s) light illumination (385 nm at 40 mW/cm^2). For HEK293T cells expressing *Kir2.1_I143$_{TAG}$* or *Kir2.1_I176$_{TAG}$*, we could detect no I_{Kir} before or after light illumination, indicating either no amber suppression or a nonfunctional channel after Cmn incorporation (Figure 2E; Figure S1C). By contrast, HEK293T cells expressing *Kir2.1_C149$_{TAG}$* displayed a large I_{Kir} that was unchanged by light illumination (Figure 2F), suggesting that incorporation of Cmn at C149 did not significantly occlude the pore. It is striking that HEK293T cells expressing *Kir2.1_C169$_{TAG}$* displayed little I_{Kir} at negative membrane potentials that increased significantly upon light illumination (Figures 2G and 2H). These results suggested that incorporation of Cmn at C169 largely occludes the channel pore and that the blocking particle is released following brief light stimulation, indicating the successful construction of a photoactivatable Kir2.1 channel.

Light-Dependent Activation of PIRK in HEK293T Cells

We next examined the light sensitivity features of Kir2.1_C169$_{TAG}$Cmn (referred to as PIRK) channels expressed in HEK293T cells. To enhance channel expression, we fused the fluorescent protein mCitrine (mCit) to the C terminus of Kir2.1_C169$_{TAG}$ (Figure 3A), which reduced the number of plasmids needed for transfection and allowed tracking the location of PIRK channels. Fusion of GFP to the C terminus of Kir2.1 was shown previously to not affect Kir2.1 channel physiology (Sekar et al., 2007). Addition of Cmn to the bath resulted in fluorescently labeled HEK293T cells (Figure 3B; Figure S2A) and the expression of full-length Kir2.1-GFP fusion protein (Figure S2B). A brief (1 s) pulse of UV light (385 nm LED, 40 mW/cm^2) led to activation of an inwardly rectifying current that was blocked by Ba^{2+} (Figures 3C and 3D). The activation kinetics had fast and slow components with time constants (τ) of 298 ± 134 ms and 15.0 ± 4.3 s, respectively (n = 7). Note that the amplitude of light-activated current is larger than that in Figure 2H, indicating that PIRK expression level increased with the two plasmid system. When incorporated with Leu, Kir2.1_C169$_{TAG}$Leu channels showed large I_{Kir} (8.30 ± 1.48 nA, n = 7), which was not affected by light illumination (data not shown). On the other hand, HEK293T cells expressing PIRK (Kir2.1_C169$_{TAG}$Cmn) channels produced no or negligible I_{Kir} before UV light (0.14 ± 0.07 nA, n = 10 versus 0.05 ± 0.02 nA, n = 9 for untransfected; $p > 0.05$, unpaired t test) and a marked increase in I_{Kir} after UV light (1.65 ± 0.41 nA, n = 10) (Figure 3E). The smaller I_{Kir} for PIRK compared to Kir2.1_C169$_{TAG}$Leu was likely due to the less efficient aminoacylation with CmnRS and, therefore, less Cmn incorporation.

To investigate the relationship between the light dosage and current activation, we varied the duration and frequency of UV light pulses. Single light pulses with different lengths were applied to cells expressing PIRK channels. Using a 40 mW/cm^2 LED light source, 1 s and 500 ms light pulses evoked similar amounts of current at −100 mV (2.27 ± 0.51 nA, n = 5 for 1 s; 2.04 ± 0.39 nA, n = 5 for 500 ms). Shorter UV pulses (200 ms, 100 ms, and 50 ms) led to progressively smaller currents (Figure 3F). No significant change in current amplitude was measured with a single 20 ms light pulse (n = 6; data not shown). We next investigated the effect of sequential UV light pulses. Sequentially delivered light pulses of 200 ms duration each led to stepwise activation of PIRK channels (Figure 3G). Fewer UV pulses were required to maximally activate PIRK channels with UV light pulses of longer duration (Figure 3H). Together, these results illustrate that modulating the duration and number of light pulses can be used to fine-tune the extent of PIRK current activation.

Light Activation of PIRK Suppresses Neuronal Firing

A significant obstacle in using Uaa technology has been the implementation of Uaa in vertebrate neurons. We therefore investigated the expression of PIRK channels in primary cultures of hippocampal neurons. Transfection of rat hippocampal primary neurons with the cDNA for PIRK-mCit and tRNA$^{Leu}_{CUA}$/CmnRS (Figure 3A) led to fluorescence in cultures exposed to Cmn for 12–48 hr (Figure 4A), indicating the successful incorporation of Cmn into PIRK channels. The expression of PIRK in neurons appeared similar to the pattern of endogenous Kir2.1 channels (Figure S3). Moreover, PIRK expression did not appear to change the basic membrane properties of the neurons (Figures S4A–S4C). Whole-cell patch-clamp recordings from mCit-positive neurons revealed no significant increase in basal inward current at negative potentials (−0.21 ± 0.06 nA, n = 6 versus −0.43 ± 0.09 nA, n = 6; $p > 0.05$, unpaired t test). However, UV light stimulation (1 s, 40 mW/cm^2) induced a large inwardly rectifying current in PIRK (+Cmn) cells (Figure 4B). By contrast, control neurons without PIRK showed little or no response to UV light (Figures 4B and 4C; Figure S4D). In PIRK-expressing neurons incubated with Cmn, UV light induced a mean inward current of −0.46 ± 0.18 nA (at −100 mV), consistent with unblock of constitutively open Kir2.1 channels (Figure 4C, Supplemental Information).

We next examined the effect of PIRK activation on the excitability of hippocampal neurons. Activation of an inwardly rectifying K^+ current would be expected to significantly reduce neuronal excitability by the outward flow of K^+ current through Kir channels (Burrone et al., 2002; Yu et al., 2004). In whole-cell current-clamp recordings, a range of current injections (range = 10–190 pA, mean ± SEM, 45 ± 4 pA, n = 56) were used to induce continuous firing of action potentials (5–15 Hz) in both control neurons and PIRK-expressing neurons (Figures 4D and 4E). The induced membrane potential was relatively consistent from cell to cell (Figure 4G). In PIRK-expressing neurons, action potential firing stopped abruptly upon brief UV light stimulation (1 s, 40 mW/cm^2). Of note, addition of Ba^{2+} to the bath restored action potential firing (Figure 4D), confirming that

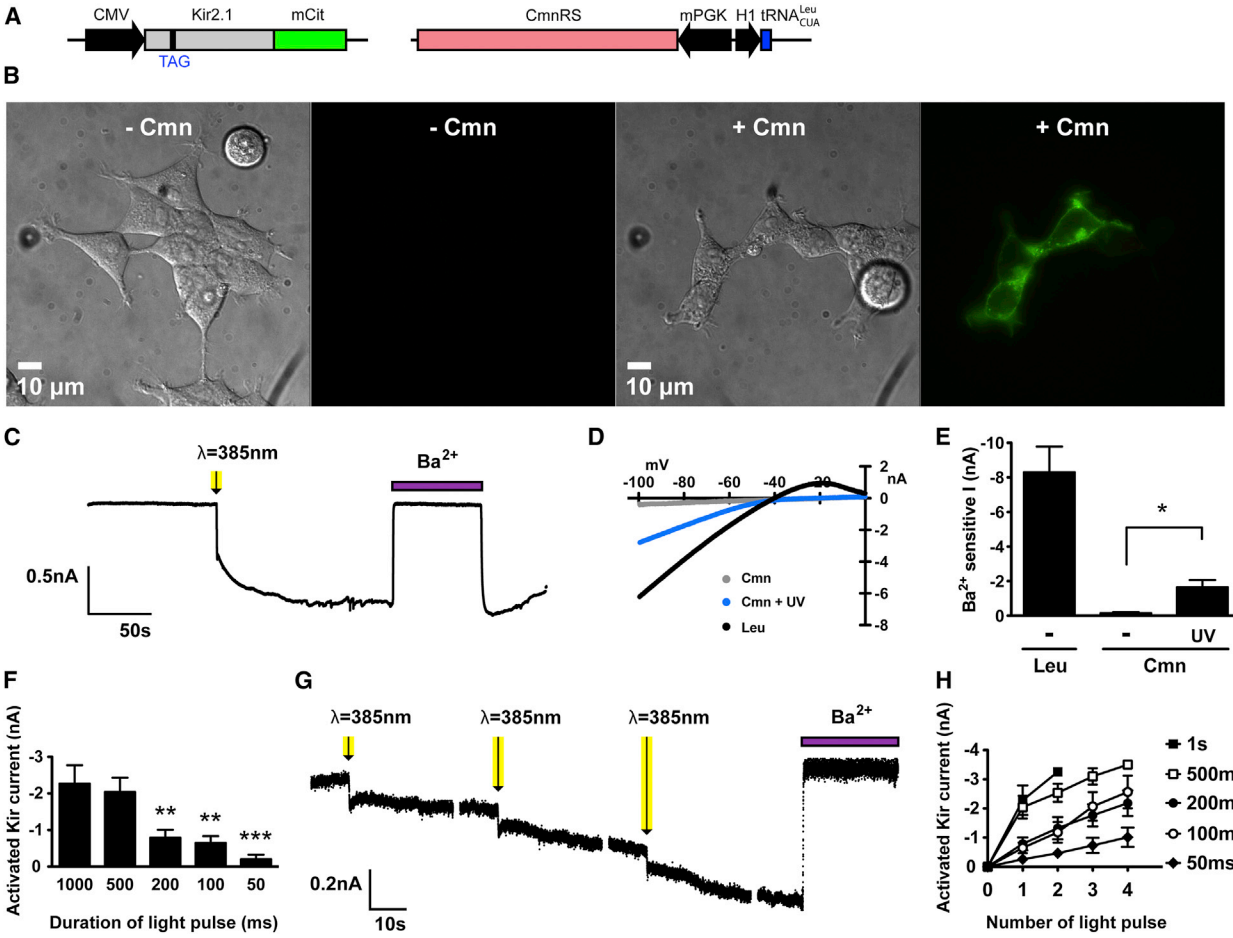

Figure 3. Light-Dependent Activation of PIRK (Kir2.1_C169$_{TAG}$Cmn) Expressed in HEK293T Cells

(A) Plasmids for PIRK expression and detection in HEK293T cells and hippocampal neurons. One plasmid encoded *Kir2.1_C169$_{TAG}$* with C-terminal fusion of *mCit* for fluorescent detection of PIRK expression, and the other plasmid encoded the tRNA$^{Leu}_{CUA}$ and *CmnRS*.

(B) Localization of PIRK channels at cell membrane. Images show PIRK-mCit expression in HEK293T cells transfected with two plasmids in (A) in the absence or presence of Cmn (1 mM) in the growth media. Differential interference contrast (DIC) and fluorescence images are shown. Note green fluorescence in +Cmn, indicating incorporation of Cmn into Kir2.1.

(C) Continuous current recording at −100 mV from HEK293T cells expressing PIRK. One second pulse of light (385 nm, 40 mW/cm^2) activated an inward current that was inhibited by extracellular $BaCl_2$ (1 mM).

(D) Photoactivated PIRK currents. The I-V plot shows the currents recorded from HEK293T cells expressing Kir2.1_C169$_{TAG}$Leu (black) and PIRK before (gray) and after (blue) light activation (385 nm, 40 mW/cm^2, 1 s).

(E) Ba^{2+}-sensitive current (I_{Kir}; mean ± SEM) measured from HEK293T cells expressing Kir2.1_C169$_{TAG}$Leu (−8.30 ± 1.48 nA, n = 7), PIRK before light activation (−0.14 ± 0.07 nA, n = 10), and PIRK after light activation (−1.65 ± 0.41 nA, n = 10). *p < 0.05, paired t test.

(F) PIRK activation was dependent on duration of light exposure. Ba^{2+}-sensitive photoactivated current was measured at −100 mV from HEK293T cells expressing PIRK after the indicated duration of light exposure (385 nm, 40 mW/cm^2). Mean currents ± SEM were as follows: 1,000 ms (−2.27 ± 0.51 nA, n = 5), 500 ms (−2.04 ± 0.39 nA, n = 5), 200 ms (−0.79 ± 0.22 nA, n = 8), 100 ms (−0.65 ± 0.18 nA, n = 8), and 50 ms (−0.20 ± 0.12 nA, n = 6). **p < 0.01 and ***p < 0.001, one-way ANOVA.

(G) Stepwise activation of PIRK following multiple light pulses. Representative current trace at −100 mV shows effect of three light pulses (200 ms each, 385 nm, 40 mW/cm^2) applied sequentially. Extracellular $BaCl_2$ (1 mM) inhibits light-activated current, confirming Kir2.1-specific current.

(H) Frequency dependence of light activation for PIRK channels. Mean Ba^{2+}-sensitive current measured at −100 mV is plotted as a function of number of light pulses (385 nm, 40 mW/cm^2) of different durations: 1,000 ms (n = 5), 500 ms (n = 5), 200 ms (n = 8), 100 ms (n = 8), and 50 ms (n = 6). Error bars represent SEM. See also Figure S2.

the observed suppression of activity was due to activation of Kir2.1 channels. Neither light illumination nor Ba^{2+} addition altered the excitability of control neurons (Figure 4E; Figures S4E and S4F). In multiple recordings from different preparations of hippocampal neuronal cultures, we consistently observed a significant decrease in firing frequency in PIRK-expressing neurons (+Cmn) following UV light, which was restored to normal levels of firing in the presence of extracellular Ba^{2+} (Figure 4F). In control neurons, we observed no significant change in firing frequency after light activation or Ba^{2+} addition (Figure 4F).

Plotting the membrane potential induced by the current step before and after UV light stimulation showed a clear hyperpolarization in PIRK-expressing (+Cmn) neurons following UV light (Figure 4G; Figure S4H). Furthermore, subsequent extracellular Ba^{2+} reproducibly depolarized the membrane potential. Taken together, these experiments demonstrate that UV light activation of PIRK channels provides a technique for spatially inhibiting neuronal activity through membrane hyperpolarization.

To explore the dynamic range of PIRK's effect on neuronal firing, we measured the firing frequency from each neuron over a range of current injections (0–70 pA). Cells that did not fire throughout the current range were excluded. With small current injections (<40 pA), the firing frequency decreased significantly upon UV light activation of PIRK channels (Figure 5A). With larger current injections (40–70 pA) and higher firing frequencies, however, there was no significant change in firing frequency following UV light illumination of PIRK-expressing neurons. This ceiling effect can be explained by the native properties of strong inwardly rectifying Kir2.1 channels, which conduct little outward current at positive membrane potentials (Ishii et al., 1994; Kubo et al., 1993). Kir channels are well known for their ability to hyperpolarize membranes and increase the threshold for firing an action potential. To examine this, we measured the minimum amount of current required to evoke an action potential (referred to as rheobase). The rheobase increased in PIRK-expressing neurons following UV light exposure (Figure 5C). UV light activation of PIRK also hyperpolarized the resting membrane potential of PIRK-expressing neurons by −17 mV, whereas UV light had no effect on the resting potential of control neurons (Figure 5D; Figure S4G).

In Vivo Expression of PIRK in the Mouse Neocortex

Having successfully expressed PIRK channels in dissociated hippocampal neurons, we next attempted to express PIRK channels in vivo. Genetically encoding Uaas using orthogonal tRNA/synthetase has great potential to address challenging biological questions in vivo, but this technology has yet to be applied in mammals. There were two main challenges for in vivo incorporation of Uaas in mammals: (1) efficient delivery and expression of the genes for the orthogonal tRNA/synthetase and the target protein into specific tissue or cells; and (2) sufficient bioavailability of the Uaa at the target tissue and cells. We chose mouse embryos for genetically incorporating Uaas into the brain because of the ability to introduce cDNA and chemicals in utero and then to prepare brain slices pre- and postnatally (Mulder et al., 2008; Saito, 2006; Tabata and Nakajima, 2001).

We started addressing the first challenge by attempting to incorporate Leu, an endogenously available amino acid, into GFP through UAG suppression in mouse embryonic brain. The GFP_Y182_{TAG} reporter gene was encoded on the same plasmid with the orthogonal $tRNA^{Leu}_{CUA}$ (Figure 6A). Three copies of this tRNA expression cassette driven by the H1 promoter were included to increase the UAG suppression efficiency, as we previously demonstrated in mammalian cells (Coin et al., 2011). A red fluorescent protein, mCherry, was coexpressed with the orthogonal LeuRS through the internal ribosome entry site (IRES) on the other plasmid to indicate successful gene delivery in vivo. Genes were introduced in the mouse neocortex using in utero electroporation, and 4 days later, the embryonic cortical sections were prepared and fluorescently imaged to check gene expression (Figure 6C). Electroporation of the LeuRS-IRES-mCherry plasmid alone showed red fluorescence, indicating that mCherry served as a good indicator for gene delivery (Figure 6D, top row). Codelivery of the $tRNA^{Leu}_{CUA}$ -GFP_{TAG} plasmid with a separate plasmid encoding mCherry showed mCherry fluorescence but no GFP fluorescence, demonstrating that there was no background readthrough of the UAG stop codon in the *GFP* mRNA (Figure 6D, middle row). On the other hand, GFP fluorescence was now observed in the neocortices of mice electroporated with $tRNA^{Leu}_{CUA}$, GFP_{TAG}, and *LeuRS* cDNA (Figure 6D, bottom row). In addition, all green fluorescent cells had red fluorescence, indicating that translation of full-length GFP required both the $tRNA^{Leu}_{CUA}$ and the LeuRS to suppress the UAG codon. Therefore, these results suggest the successful in vivo incorporation of Leu into GFP through UAG suppression.

Incorporation of a Uaa in vivo presented an additional challenge. For the convenience of detection, we initially tried to incorporate Cmn into GFP_{TAG} in the mouse brain using a heterochronic approach. The $tRNA^{Leu}_{CUA}$, *CmnRS*, and GFP_{TAG} genes (Figure 6A) were first electroporated in utero, and then after 2 days, we injected Uaa Cmn directly into the lateral ventricle of the mouse brain (Figure 6C). Without injecting Cmn, no green fluorescence was detected in the neocortical plates (Figure 6E, top row). After injection of Cmn, weak green fluorescence could be detected (data not shown). Previously, we discovered that preparation of Uaa in the dipeptide form increases the efficiency of Uaa incorporation in *C. elegans*, possibly because the dipeptide is transported into cells more efficiently than the single Uaa via oligopeptide transporters PEPT1 and PEPT2 (Parrish et al., 2012). Intracellular dipeptide would then be hydrolyzed by cellular peptidases to generate the free Uaa for incorporation. Since PEPT2 is highly expressed in rodent brain (Lu and Klaassen, 2006), Cmn-alanine (Cmn-Ala) was adopted to improve Cmn bioavailability. We thus synthesized the Cmn-Ala dipeptide and injected it in the lateral ventricle of the mouse brain. Indeed, with this adjustment, we could observe a dramatic improvement, with strong green fluorescence in the neocortex (Figure 6E, bottom row), indicating the successful incorporation of Cmn into GFP_{TAG} in vivo.

After overcoming both challenges, we proceeded to incorporate Cmn into $Kir2.1\_C169_{TAG}$ to express PIRK channels directly in the mouse brain. The $Kir2.1\_C169_{TAG}$ gene was encoded with the $tRNA^{Leu}_{CUA}$ in one plasmid, and another plasmid encoded the *CmnRS* together with *mCherry* as a reporter for gene delivery (Figure 6B). A third plasmid encoding GFP_Y182_{TAG} was also coelectroporated in utero. Detection of GFP fluorescence would indicate the successful delivery of all three plasmids, since UAG suppression in GFP would require both the $tRNA^{Leu}_{CUA}$ and the CmnRS; Cmn incorporation in GFP_{TAG} would suggest Cmn incorporation in $Kir2.1_{TAG}$ as well, because both genes were present in the same cell. As expected, only when all three gene constructs were present and Cmn-Ala was introduced to the brain, green fluorescent cells were observed in the mouse neocortex (Figure 6F). Cells with both red and green fluorescence should have Cmn incorporated into $Kir2.1_{TAG}$ to make PIRK channels.

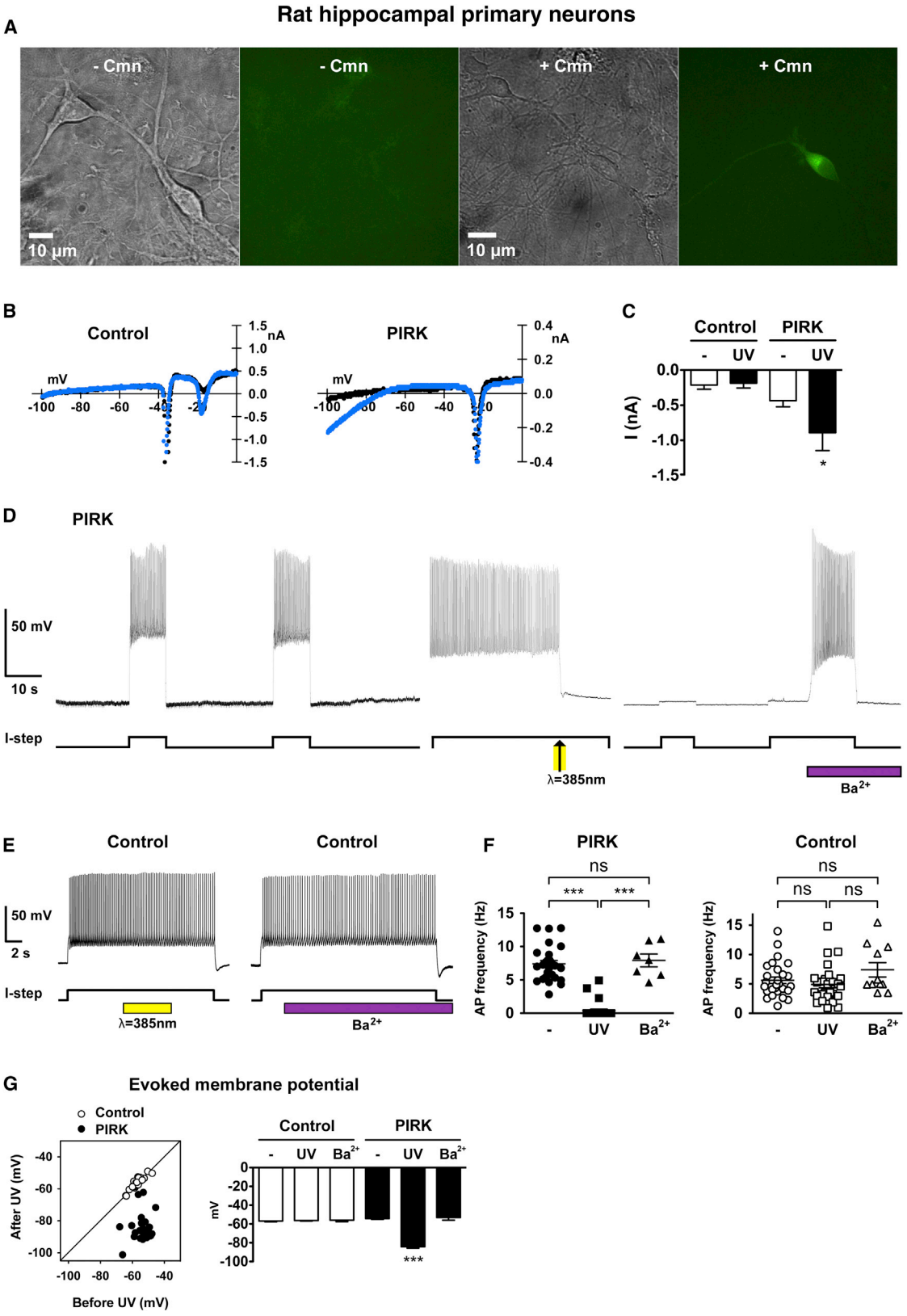

(legend on next page)

To verify if functional PIRK channels were expressed in these neurons, we conducted whole-cell recordings on acute slices prepared from the mouse neocortical plates. Indeed, the green and red fluorescent neurons had no inward current at negative holding potential, but a brief pulse of light rapidly activated the inward current (Figure 6G). The current was completely blocked by adding Ba^{2+}, confirming that it was generated by PIRK. In contrast, control neurons did not show any photoactivated inward current (Figures S5C and S5D). I_{kir} measured from these PIRK-expressing neurons in the mice neocortical slices was significantly increased upon light activation (Figure 6H). The light-dependent activation of PIRK channels further confirmed the successful incorporation of Cmn into $Kir2.1_{TAG}$ in the mouse brain. In short, these data demonstrate the successful expression of a functional PIRK in vivo.

To demonstrate the general utility of this technique for other brain regions, we also performed in utero electroporation and in utero injection of Uaas in embryonic diencephalon that included thalamus and hypothalamus. The procedure was similar to that described earlier for the neocortex, but it involved a heterochronic procedure with an injection of the $tRNA^{Leu}_{CUA}$-GFP_{TAG} plasmid and CmnRS-IRES-mCherry plasmid (Figure 6A) into the third ventricle at embryonic day 13.5 (E13.5) accompanied by electroporation, then later at E16.5 an injection of Cmn-Ala into or near to the third ventricle. The embryos were harvested at E17.5, and the brains were analyzed using imaging methods. GFP expression is clearly evident, indicating Uaa incorporation into GFP_{TAG} (Figures S5E and S5F).

DISCUSSION

Genetically encoding Uaas with orthogonal tRNA/synthetase was initially developed in *E. coli* and later extended to various single cells and, recently, to invertebrates such as *Caenorhabditis elegans* (Liu and Schultz, 2010; Parrish et al., 2012; Wang et al., 2001, 2009). For neuroscience research, Uaa incorporation in primary neurons (Wang et al., 2007), neural stem cells (Shen et al., 2011), and animals would permit the use of Uaas in directly addressing neurobiological processes in the native environment. Previously, Uaas have been incorporated into ion channels and receptors expressed in *Xenopus oocytes* (Beene et al., 2003) and mammalian cells in vitro (Wang et al., 2007). Although sufficient for probing the structure and function of a single target protein, heterologous expression systems are not suitable for investigating neuronal signaling and circuits involving a cascade of neuronal proteins or multiple cells. In this report, we describe the methodology for manipulating a neuronal protein directly in primary neurons using genetically encoded Uaas. Moreover, we report the successful incorporation of Uaas into the brain of mouse embryos, effectively expanding the genetic code of mammals. To overcome the obstacles for Uaa incorporation in vivo, we delivered the genes for the orthogonal tRNA/synthetase into mouse neocortex and diencephalon by in utero electroporation and supplied the Uaa to the brain in the form of a dipeptide through injection to the ventricles. The ability to genetically incorporate Uaas into neuronal proteins in mammalian brains provides a novel toolbox for innovative neuroscience research.

The development of optically controlled channels and pumps is a powerful method for analyzing the function of specific neurons in neural circuits (Yizhar et al., 2011). However, the photoresponsiveness of opsin, which depends on the retinal chromophore and its modulation protein domain, cannot be simply transplanted into other proteins without dramatically altering the target protein. Therefore, this approach is not suitable for optical control of proteins natively expressed in neurons. Alternatively, natively expressed channels and receptors can be modified to be controlled by an optically switched ligand. For example, a photoisomerizable azobenzene-coupled ligand can be chemically attached to the glutamate receptor sGluR0 or

Figure 4. Light Activation of PIRK Suppresses Firing of Rat Hippocampal Neurons

(A) DIC and fluorescence images of rat hippocampal neurons cultured in vitro and transfected with *PIRK* fused to *mCit* and $tRNA^{Leu}_{CUA}$/*CmnRS* (plasmids shown in Figure 3A) in the absence or presence of Cmn (1 mM) in the growth media. Note green fluorescence in +Cmn, indicating incorporation of Cmn.

(B) PIRK-expressing neurons showed photoactivated inward current. I-V plots produced with a voltage-ramp protocol for a control neuron and a neuron expressing PIRK before (black) and after (blue) illumination (385 nm, 40 mW/cm^2, 1 s). Note inwardly rectifying current negative to −70 mV. Rapid downward deflections likely reflect action potentials.

(C) Selective photoactivation of current in PIRK-expressing neurons. Currents (mean ± SEM) were measured at −100 mV before (open column) and after (filled column) illumination (385 nm, 40 mW/cm^2, 1 s): control neurons (before, −0.21 ± 0.06 nA; after, −0.19 ± 0.07 nA, n = 6); PIRK-expressing neurons (before, −0.43 ± 0.09 nA; after, −0.89 ± 0.25 nA, n = 6). *$p < 0.05$, paired t test. Currents are not leak-subtracted.

(D) A single light pulse suppressed firing of a hippocampal neuron expressing PIRK. Representative voltage traces recorded continuously in current-clamp. Maximal firing was evoked by 20 pA current injection (I-step). Light exposure (385 nm, 40 mW/cm^2, 1 s; indicated with arrow) rapidly and completely suppressed neuronal firing. Firing was restored with extracellular 500 μM $BaCl_2$, which selectively inhibits Kir2.1 channels.

(E) Neither UV illumination alone nor $BaCl_2$ (500 μM) altered excitability of control neurons. Maximal firing was evoked by 50 pA current injection (I-step).

(F) Plot of action potential frequency of PIRK-expressing and control neurons before light, after light activation, and following application of Ba^{2+}. One second of a 385 nm light pulse at 40 mW/cm^2 was applied for activation. Maximal firing was elicited by a single current step (45 ± 4 pA, n = 56). Mean firing frequencies ± SEM for PIRK-expressing neurons were as follows: before UV, 7.4 ± 0.5 Hz, n = 28; after UV, 0.4 ± 0.2 Hz, n = 28; and after Ba^{2+} addition, 7.9 ± 1.0 Hz, n = 7. Values for control neurons were as follows: before UV, 5.6 ± 0.6 Hz, n = 28; after UV, 4.9 ± 0.6 Hz, n = 28; after Ba^{2+} addition, 7.4 ± 1.2 Hz, n = 11. ***$p < 0.001$, one-way ANOVA.

(G) Light activation significantly hyperpolarized PIRK-expressing neurons. One second of 385 nm light pulse at 40 mW/cm^2 was applied for activation. Membrane potential was measured at the evoked state, as in (D), after current injection. Left: the membrane potential after light activation is plotted as a function of membrane potential before light activation for each cell (PIRK-expression neurons: filled circle, n = 28; control neurons: open circle, n = 28). Right: membrane potential measured under indicated conditions was plotted. Mean values ± SEM are given for control neurons (before UV, −57 ± 1 mV, n = 28; after UV, −56 ± 1 mV, n = 28; and after 500 μM $BaCl_2$ addition, −56 ± 2 mV, n = 8) and for PIRK-expressing neurons (before UV, −54 ± 1 mV, n = 28; after UV, −84 ± 2 mV, n = 28; and after 500 μM $BaCl_2$, −53 ± 3 mV, n = 7). ***$p < 0.001$, one-way ANOVA.

See also Figures S3 and S4.

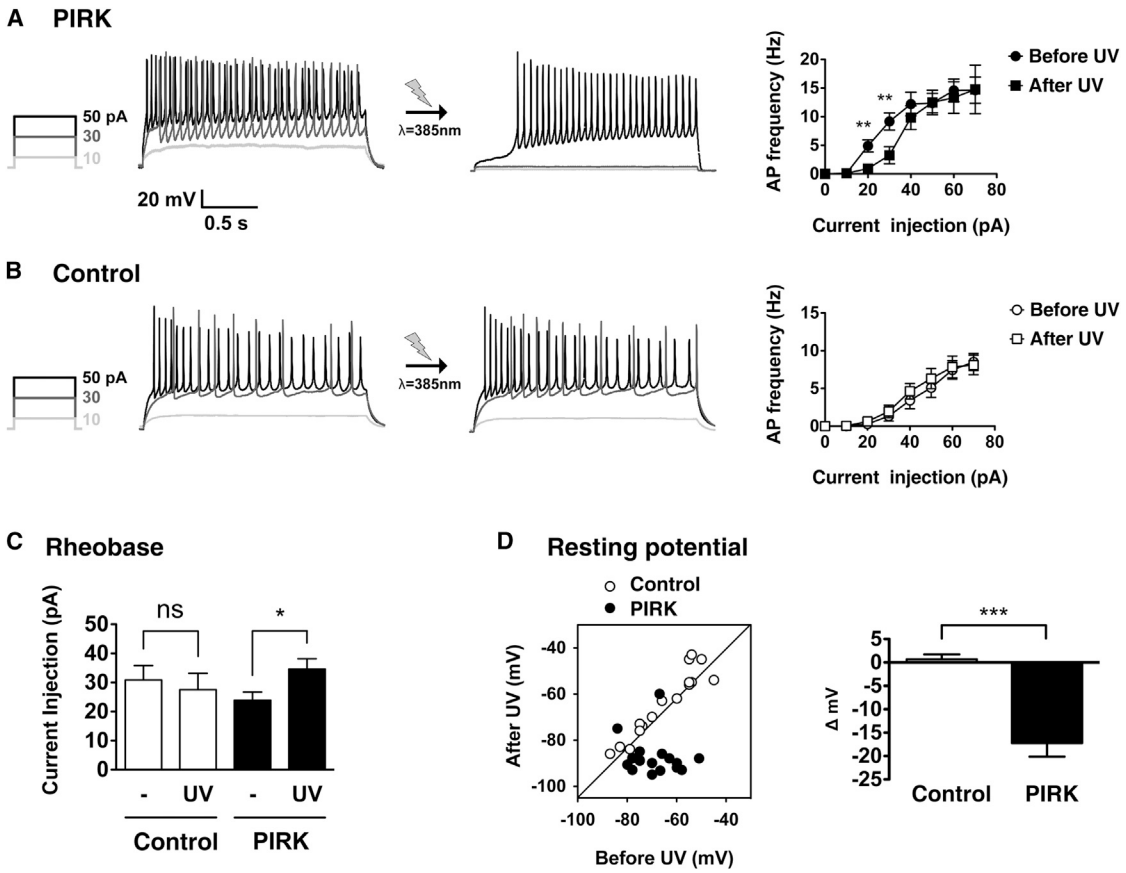

Figure 5. Dynamic Range of PIRK-Dependent Suppression of Neuronal Firing

(A) In PIRK-expressing hippocampal neurons, photoactivation of PIRK significantly decreased action potential firing frequency, dependent on current injection amplitude. Representative voltage traces in response to three step-current injections (10 [light gray], 30 [dark gray], and 50 [black] pA) before (left) and after (right) light exposure (385 nm, 40 mW/cm^2, 1 s). Graph shows mean action potential frequency plotted as a function of current injection amplitude (n = 13). **p < 0.01, paired t test. Error bars represent SEM.

(B) In control neurons, light exposure had no effect on action potential frequency. Representative voltage traces in response to three step-current injections (10 [light gray], 30 [dark gray], and 50 [black] pA) before (left) and after (right) light exposure (385 nm, 40 mW/cm^2, 1 s). Graph shows mean action potential frequency plotted as a function of current injection amplitude (n = 12). Error bars represent SEM.

(C) Rheobase, the minimum current required to fire an action potential, significantly increased in PIRK-expressing neurons upon light activation (385 nm, 40 mW/cm^2, 1 s). Mean rheobase values (mean ± SEM) are given for control neurons (before UV, 31 ± 5 pA; after UV, 28 ± 6 pA; n = 12) and for PIRK-expressing neurons (before UV, 24 ± 3 pA; after UV, 35 ± 4 pA; n = 13). *p < 0.05, paired t test.

(D) Resting membrane potential of PIRK-expressing neurons shifted to negative potentials upon light activation (385 nm, 40 mW/cm^2, 1 s). Left: the resting potential after light activation is plotted as a function of the resting potential before light activation for each cell (PIRK-expressing neurons: solid circle, n = 19; control neurons: open circle, n = 19). Right: bar graph shows light-induced shift in resting potential. Specific values (mean ± SEM) of ΔmV were as follows: control neurons, 1 ± 1 mV, n = 19; PIRK-expressing neurons, −17 ± 3 mV, n = 19. ***p < 0.001, unpaired t test.

See also Figure S4.

the potassium channel TREK1 for light gating (Janovjak et al., 2010; Sandoz et al., 2012). A limitation with this technique, however, is that application of the chemical photoswitch has been described for labeling extracellular regions of the target protein, suggesting that intracellular proteins may be less amenable to this labeling method. In contrast, genetically encoding photoreactive Uaas should provide a general methodology for manipulating neuronal proteins, both cytoplasmic and membrane proteins, with light in neurons. Since genetic incorporation of Uaas using orthogonal tRNA/synthetase pairs imposes no restrictions on target protein type, cellular location, or the site for Uaa incorporation (Wang and Schultz, 2004), with methods reported herein, we expect that various proteins expressed in neurons can be generally engineered with photoreactive Uaas at an appropriate site to enable optical control. Moreover, a family of photoreactive Uaas exist (Beene et al., 2003; Liu and Schultz, 2010) that can be fine-tuned for a particular active site in the protein. This flexibility should significantly expand the scope of proteins and neuronal processes subject to light regulation.

Photoactivation of PIRK channels expressed in hippocampal neurons led to constitutive activation of Kir2 channels that produced a sustained suppression of neuronal firing. There are unique features of PIRK that may complement existing methods

for neuronal silencing. Archaeorhodopsin-3 (Arch) and halorhodopsin (NpHR) are members of the opsin family used to silence neuronal activity (Chow et al., 2010; Zhang et al., 2007). Illumination of Arch, a proton pump, for an extended period of time could result in intra- and extracellular pH disturbance, which could negatively impact on cell health (Han, 2012; Okazaki et al., 2012). Activation of the chloride pump NpHR leads to accumulation of intracellular chloride ions and can compromise $GABA_A$-receptor-mediated inhibition (Raimondo et al., 2012). In addition, continuous activation of Arch or NpHR is limited by its inactivation and potential photo damage, which is not ideal for studies, such as those researching epilepsy, in which it is important to maintain membrane hyperpolarization for a long period of time (Kokaia et al., 2013). In contrast, PIRK is based on Kir2.1, an inward rectifying potassium channel whose native function is to regulate neuronal excitability (Bichet et al., 2003; Hibino et al., 2010; Nichols and Lopatin, 1997). Through a small amount of outward K^+ current, Kir2.1 can directly silence the electrical activity of neurons. In fact, ectopic expression of Kir channels has been used previously over the last decade to investigate the effect of neuronal excitability on circuit function (Burrone et al., 2002; Johns et al., 1999; Nadeau et al., 2000; Yu et al., 2004). By endowing Kir2.1 with photoresponsiveness in PIRK, we have provided the ability to temporally control through light precision the activation of Kir2 channels. Another advantage of PIRK is that it functions like a binary switch, whereby a single light pulse can induce the lasting silencing effect on target neurons. Without the need to continuously deliver light through the optical fiber, this binary switch feature of PIRK is convenient for animal studies to mitigate potential interference of light or light devices on animal behavior and could, therefore, be useful for studying or treating intractable epilepsy, intractable pain, or muscle spasms. Moreover, PIRK channels may be utilized for studying a variety of physiological processes and diseases that directly involve Kir2.1 channels. For example, Kir2.1 function has been implicated in Andersen syndrome (Plaster et al., 2001), cardiac short QT syndrome (Priori et al., 2005), and osteoblastogenesis (Zaddam et al., 2012).

PIRK is designed with a photoreleasable pore-blocking group. This ''block-and-release'' strategy may be generally applicable to other channels and receptors. For instance, G protein-gated Kir channels (Kir3 family), α-amino-3-hydroxy-5-methyl-4-isoxazolepropionic acid receptors, and *N*-Methyl-D-aspartic acid receptors share similar pore topology with Kir2.1. By incorporating Cmn into pore residues in these proteins, one should be able to similarly install in light responsiveness to them for highly disciplined study of channel/receptor physiology. On a broader perspective, it is also possible to expand the Uaa-based optical control to the function of other proteins beyond ion channels and receptors. Multiple amino acids such as tyrosine, serine, lysine, glutamate, aspartate, and glycine have been caged with different photoreleasable groups (Beene et al., 2003), and some of them can be genetically encoded in *E. coli*, yeast, and mammalian cells (Liu and Schultz, 2010; Wang et al., 2009). Using methods described in this report, these amino acids can be similarly photocaged for optical control of various protein functions in neurons. For instance, by photocaging appropriate amino acids, it should be possible to block and release protein-protein interaction, protein-nucleic acid interaction, access of an active site, or access of posttranslational modification sites in neurons. In addition, in vivo Uaa incorporation, as demonstrated in the embryonic mouse neocortex and diencephalon here, has the potential to be extended to other regions of the brain, adult animals, and more mammals. Genetic knockin or viral delivery (Shen et al., 2011) can be used to express the orthogonal tRNA/synthetase and target protein in transgenic and adult animals, respectively. Some Uaas may be bioavailable through food or water feeding; others can be prepared in the dipeptide format shown here and injected directly into the brain ventricles. Moreover, optical control via Uaa can be made compatible with two-photon activation. Protecting groups efficient for two-photon photolysis have been developed for caging amino acids (Matsuzaki et al., 2001). In the future, it may be possible to genetically incorporate azobenzene-containing Uaas into neurons for reversible optical control (Bose et al., 2006). In summary, the methodology presented here serves as a solid basis for optically controlling a variety of neuronal proteins in studies of neurobiological processes in the brain.

EXPERIMENTAL PROCEDURES

Electrophysiology and Light Activation in Culture

A whole-cell patch clamp was used to record macroscopic currents with an Axopatch 200B (Molecular Devices, Axon Instruments) amplifier. Currents were adjusted electronically for cell capacitance and series resistance (80%–100%), filtered at 1 kHz with an eight-pole Bessel filter and digitized at 5 kHz with a Digidata 1200 interface (Molecular Devices). For voltage-clamp recordings, currents were elicited with a voltage ramp from −100 mV to 50 mV delivered at 0.5 Hz. For some recordings, cells were held at −100 mV continuously. For current-clamp recordings, the resting potential was first adjusted to around −72 mV by injecting small current. Afterward, a step current was injected to induce continuous firing (5–15 Hz) of action potentials. For Cmn photolysis, an LED with an emission of 385 nm (~40 mW; Prizmatix) was externally installed at the microscope to deliver light to the cell from 1 cm away at a 45° angle. Light power at the sample measured 40 mW/cm^2. Light pulse was signaled from the amplifier through the digitizer. Data are expressed as mean ± SEM, and statistical significances ($p < 0.05$) were determined by one-way ANOVA with a Newman-Keuls test or Student's t test. All measurements were made at room temperature.

In Utero Electroporation and In Utero Injection of Uaas

Introduction of plasmid DNA into the neuroepithelial cells of mouse embryonic neocortex in utero was performed as described elsewhere (Tabata and Nakajima, 2001), with minor modifications. In brief, the uterine horns were exposed at E14.5, and ~1 μl DNA solution (0.2–5 μg/μl of each plasmid, depending on the construct) was injected into the lateral ventricle of each littermate. Embryos were then electroporated with an electroporator CUY21EDIT (BEX, 0.5 cm puddle type electrode, 33–35 V, 50 ms duration, four to eight pulses). After electroporation, the uterine horns were returned to the abdominal cavity to allow the embryos to continue development. For Leu incorporation (Figure 6D), the embryos were harvested 4 days after electroporation, and the brains were then subjected to the imaging analysis. For Cmn incorporation (Figures 6E–6H), the uterine horns were exposed again at E16.5, and Cmn (500 mM, 2–5 μl) was injected to the electroporated side or both sides of the lateral ventricle. The uterine horns were placed back into the abdominal cavity again. Twelve to forty-eight hours after Cmn injection, the embryos were harvested, and the brains were then subjected to the imaging analysis or electrophysiology as described later. For imaging analysis, the brains were fixed with 4% paraformaldehyde in PBS at 4°C for 2–4 hr. After equilibration with 30% (w/v) sucrose in PBS, the fixed brains were embedded in optimal cutting temperature compound (Sakura) and frozen. Coronal sections (10 μm thick) were

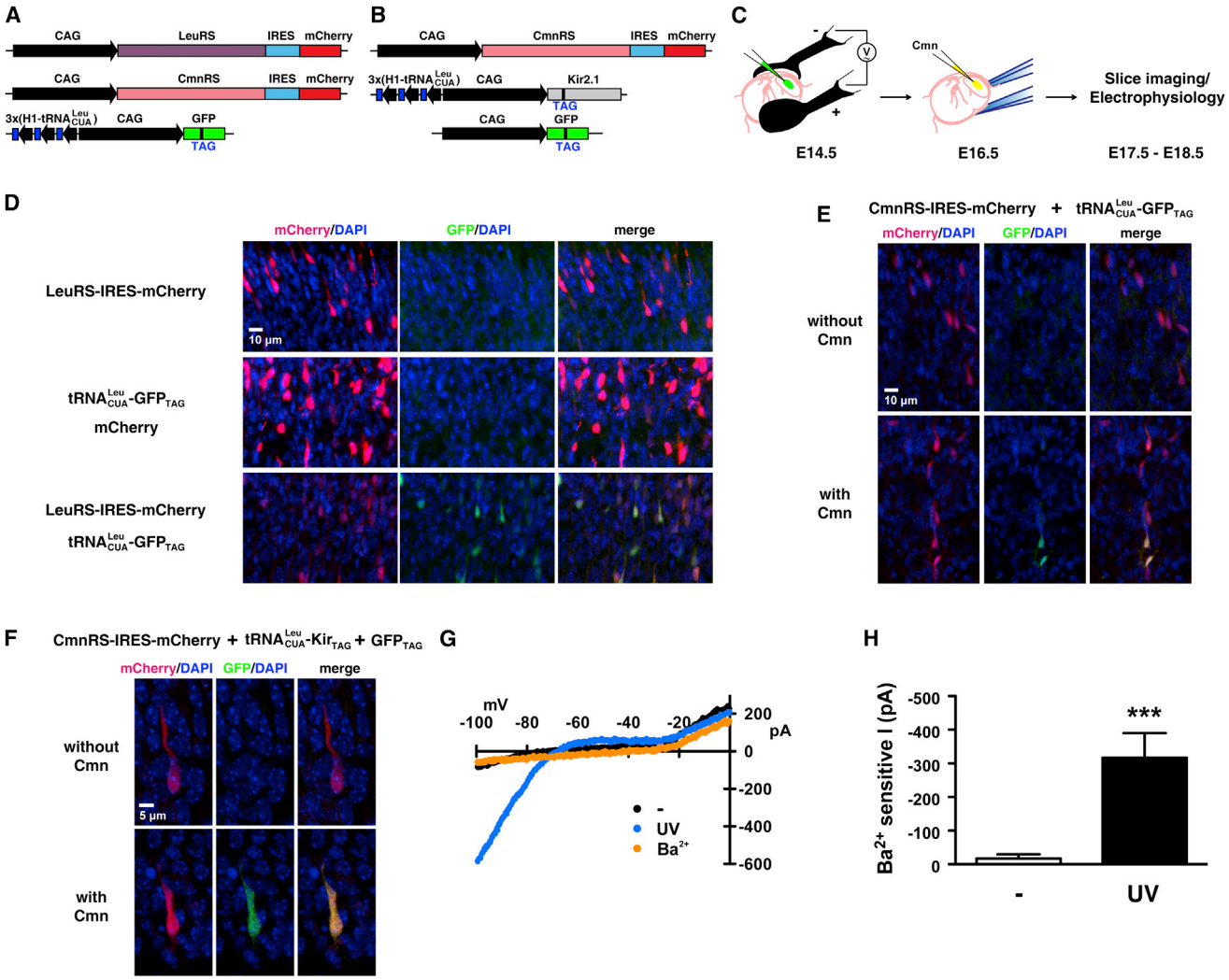

Figure 6. In Vivo Expression of PIRK Channels in the Mouse Neocortex

(A) Validation plasmid set: one plasmid for *LeuRS* or for *CmnRS*, under the control of CAG promoter and coexpressed with *mCherry* via IRES sequence; one plasmid encoding *GFP_Y182*$_{TAG}$ under the control of the CAG promoter. Three copies of tRNA$^{Leu}_{CUA}$ driven by the H1 promoter were combined with the *GFP_Y182*$_{TAG}$ to increase incorporation efficiency. Green fluorescence indicates suppression of amber codon by Leu or Cmn. Red fluorescence indicates successful gene delivery of synthetase in vivo.

(B) PIRK expression plasmid set: one plasmid for *CmnRS*, under the control of CAG promoter and coexpressed with *mCherry* via IRES sequence; one plasmid for *Kir2.1_C169*$_{TAG}$ coupled with three copies of tRNA$^{Leu}_{CUA}$; one plasmid for *GFP_Y182*$_{TAG}$. Green and red fluorescence indicates successful expression of all three plasmids and Cmn incorporation.

(C) Cartoon shows experimental procedure for PIRK expression in vivo. Gene constructs in (B) were injected into the mouse neocortex (E14.5) and electroporated in utero. Two days later, Cmn was injected to the brain. Slice imaging and electrophysiological assay were performed on E17.5–E18.5.

(D) Fluorescence images of mice embryonic cortical plates showing the successful incorporation of Leu into GFP$_{TAG}$ in vivo. Top: CAG-LeuRS-IRES-mCherry only. Middle: 3x(H1tRNA$^{Leu}_{CUA}$)-CAG-GFP$_{TAG}$, with CAG-mCherry as an injection marker. Bottom: CAG-LeuRS-IRES-mCherry and 3x(H1tRNA$^{Leu}_{CUA}$)-CAG-GFP$_{TAG}$. Fluorescence of mCherry and GFP was imaged in separate channels, shown with DAPI staining of DNA, and merged in the right column. GFP fluorescence was detected only when the tRNA$^{Leu}_{CUA}$, *LeuRS*, and *GFP_Y182*$_{TAG}$ were all present. Leu is present in vivo all the time.

(E) Fluorescence images of mice embryonic cortical plates showing the successful incorporation of Cmn into GFP$_{TAG}$ in vivo. CAG-CmnRS-IRES-mCherry and 3x(H1tRNA$^{Leu}_{CUA}$)-CAG-GFP$_{TAG}$ were electroporated in utero in both rows. The Uaa Cmn (in the form of Cmn-Ala dipeptide) was injected in utero as shown in the bottom row but not in the top row. GFP fluorescence was detected in neurons only when the tRNA$^{Leu}_{CUA}$, *CmnRS*, *GFP_Y182*$_{TAG}$, and Cmn were all present.

(F) Fluorescence images of mice embryonic cortical neurons showing the incorporation of Cmn into GFP$_{TAG}$ and Kir2.1$_{TAG}$ in vivo. The three gene constructs in (B) were electroporated in utero. GFP fluorescence was detected only with Cmn injection (bottom), indicating Cmn incorporation in GFP$_{TAG}$ and likely Cmn incorporation in the Kir2.1$_{TAG}$.

(G) I-V plot of currents recorded from mice neocortical neurons showing light-dependent activation of PIRK. Two days after gene constructs in (B) were electroporated, Cmn was injected in utero; 12-48 hr after Cmn injection, neocortical acute slices were prepared from the embryos, as in (C). PIRK-expressing neurons

(legend continued on next page)

prepared by cutting the frozen brains with a cryostat CM3050S (Leica), and the fluorescence of GFP and mCherry was detected using microscopies. DAPI (Sigma) was used to counterstain nuclei.

Electrophysiology and Light Activation in Acute Slices

After in utero electroporation and Cmn delivery, E17.5–E18.5 mice embryos were harvested, and sagittal slices (200 μm) from their neocortices were prepared in ice-cold artificial cerebral spinal fluid (ACSF) (119 mM NaCl, 2.5 mM KCl, 1.3 mM $MgCl_2$, 2.5 mM $CaCl_2$, 1 mM NaH_2PO_4, 26.2 mM $NaHCO_3$, and 11 mM glucose, pH 7.3) continuously bubbled with 95%/5% O_2/CO_2. Vibratome slices were warmed to 33°C and incubated for 42 min in ACSF supplemented with 3 mM *myo*-inositol, 0.4 mM ascorbic acid, and 2 mM sodium pyruvate and then transferred to the recording chamber superfused with ACSF (2 ml/min).

Neurons were visualized with a Hamamatsu digital camera (Model C8484) on an Olympus microscope (BX51WI), and whole-cell patch-clamp recordings (Axopatch 200B) were made from neurons in the neocortex. PIRK-expressing neurons were identified by GFP and mCherry fluorescence. The internal solution contained 130 mM potassium gluconate, 4 mM $MgCl_2$, 5 mM HEPES, 1.1 mM EGTA, 3.4 mM Na_2ATP, 10 mM sodium creatine phosphate, and 0.1 mM Na_3GTP at pH 7.3 with KOH. $BaCl_2$ (0.5 mM) was diluted into ACSF and applied directly on to the slice. Currents were elicited with a voltage ramp protocol from −100 mV to 50 mV. For Cmn photolysis, an LED with emission of 385 nm (≥190 mW; Prizmatix) was installed at the microscope to deliver light through the objective. Light power that reached the samples was measured to be 8 mW/cm^2. Electrophysiological chemicals were purchased from Sigma-Aldrich or Tocris Bioscience. Data are expressed as mean ± SEM, and statistical significances ($p < 0.05$) were determined by Student's t test. All measurements were made at ~33°C.

SUPPLEMENTAL INFORMATION

Supplemental Information includes Supplemental Experimental Procedures and five figures and can be found with this article online at http://dx.doi.org/10.1016/j.neuron.2013.08.016.

ACKNOWLEDGMENTS

We thank Dr. Michael Hausser for helpful discussions. I.C. was supported by a Marie Curie fellowship from the European Commission within the Seventh Framework Programme. D.K. and D.D.M.O. are supported by the National Institutes of Health (R01NS31558 and R01MH086147). L.W. acknowledges support from The Salk Innovation Grant, the California Institute for Regenerative Medicine (RN1-00577-1), and the National Institutes of Health (1DP2OD004744-01 and P30CA014195).

Accepted: August 9, 2013
Published: October 16, 2013

REFERENCES

Adams, S.R., and Tsien, R.Y. (1993). Controlling cell chemistry with caged compounds. Annu. Rev. Physiol. *55*, 755–784.

Beene, D.L., Dougherty, D.A., and Lester, H.A. (2003). Unnatural amino acid mutagenesis in mapping ion channel function. Curr. Opin. Neurobiol. *13*, 264–270.

Bernstein, J.G., and Boyden, E.S. (2011). Optogenetic tools for analyzing the neural circuits of behavior. Trends Cogn. Sci. *15*, 592–600.

Bichet, D., Haass, F.A., and Jan, L.Y. (2003). Merging functional studies with structures of inward-rectifier K(+) channels. Nat. Rev. Neurosci. *4*, 957–967.

Bose, M., Groff, D., Xie, J., Brustad, E., and Schultz, P.G. (2006). The incorporation of a photoisomerizable amino acid into proteins in E. coli. J. Am. Chem. Soc. *128*, 388–389.

Burrone, J., O'Byrne, M., and Murthy, V.N. (2002). Multiple forms of synaptic plasticity triggered by selective suppression of activity in individual neurons. Nature *420*, 414–418.

Chow, B.Y., Han, X., Dobry, A.S., Qian, X., Chuong, A.S., Li, M., Henninger, M.A., Belfort, G.M., Lin, Y., Monahan, P.E., and Boyden, E.S. (2010). High-performance genetically targetable optical neural silencing by light-driven proton pumps. Nature *463*, 98–102.

Coin, I., Perrin, M.H., Vale, W.W., and Wang, L. (2011). Photo-cross-linkers incorporated into G-protein-coupled receptors in mammalian cells: a ligand comparison. Angew. Chem. Int. Ed. Engl. *50*, 8077–8081.

Dart, C., Leyland, M.L., Spencer, P.J., Stanfield, P.R., and Sutcliffe, M.J. (1998). The selectivity filter of a potassium channel, murine kir2.1, investigated using scanning cysteine mutagenesis. J. Physiol. *511*, 25–32.

England, P.M., Lester, H.A., Davidson, N., and Dougherty, D.A. (1997). Site-specific, photochemical proteolysis applied to ion channels in vivo. Proc. Natl. Acad. Sci. USA *94*, 11025–11030.

Fehrentz, T., Schönberger, M., and Trauner, D. (2011). Optochemical genetics. Angew. Chem. Int. Ed. Engl. *50*, 12156–12182.

Fenno, L., Yizhar, O., and Deisseroth, K. (2011). The development and application of optogenetics. Annu. Rev. Neurosci. *34*, 389–412.

Han, X. (2012). In vivo application of optogenetics for neural circuit analysis. ACS Chem. Neurosci. *3*, 577–584.

Hibino, H., Inanobe, A., Furutani, K., Murakami, S., Findlay, I., and Kurachi, Y. (2010). Inwardly rectifying potassium channels: their structure, function, and physiological roles. Physiol. Rev. *90*, 291–366.

Ishii, K., Yamagishi, T., and Taira, N. (1994). Cloning and functional expression of a cardiac inward rectifier K+ channel. FEBS Lett. *338*, 107–111.

Janovjak, H., Szobota, S., Wyart, C., Trauner, D., and Isacoff, E.Y. (2010). A light-gated, potassium-selective glutamate receptor for the optical inhibition of neuronal firing. Nat. Neurosci. *13*, 1027–1032.

Johns, D.C., Marx, R., Mains, R.E., O'Rourke, B., and Marbán, E. (1999). Inducible genetic suppression of neuronal excitability. J. Neurosci. *19*, 1691–1697.

Kokaia, M., Andersson, M., and Ledri, M. (2013). An optogenetic approach in epilepsy. Neuropharmacology *69*, 89–95.

Kubo, Y., Baldwin, T.J., Jan, Y.N., and Jan, L.Y. (1993). Primary structure and functional expression of a mouse inward rectifier potassium channel. Nature *362*, 127–133.

Kubo, Y., Yoshimichi, M., and Heinemann, S.H. (1998). Probing pore topology and conformational changes of Kir2.1 potassium channels by cysteine scanning mutagenesis. FEBS Lett. *435*, 69–73.

Lemke, E.A., Summerer, D., Geierstanger, B.H., Brittain, S.M., and Schultz, P.G. (2007). Control of protein phosphorylation with a genetically encoded photocaged amino acid. Nat. Chem. Biol. *3*, 769–772.

Liu, C.C., and Schultz, P.G. (2010). Adding new chemistries to the genetic code. Annu. Rev. Biochem. *79*, 413–444.

Lu, H., and Klaassen, C. (2006). Tissue distribution and thyroid hormone regulation of Pept1 and Pept2 mRNA in rodents. Peptides *27*, 850–857.

in the slices, detected by both red and green fluorescence, were recorded before (black) and after (blue) light exposure (385 nm, 8 mW/cm^2, 10 s for saturated exposure). $BaCl_2$ (500 μM) was added to verify I_{Kir} after photoactivation (orange).
(H) Ba^{2+}-sensitive current (I_{Kir}) measured from PIRK-expressing neurons in mice neocortical slices showed significant increase upon photoactivation. Mean I_{Kir} ± SEM at −100 mV was as follows: before light exposure, −17 ± 13 pA; after light exposure, −317 ± 73 pA; n = 15. ***$p < 0.001$, paired t test.
See also Figure S5.

Lu, T., Nguyen, B., Zhang, X., and Yang, J. (1999a). Architecture of a K+ channel inner pore revealed by stoichiometric covalent modification. Neuron *22*, 571–580.

Lu, T., Zhu, Y.G., and Yang, J. (1999b). Cytoplasmic amino and carboxyl domains form a wide intracellular vestibule in an inwardly rectifying potassium channel. Proc. Natl. Acad. Sci. USA *96*, 9926–9931.

Matsuzaki, M., Ellis-Davies, G.C., Nemoto, T., Miyashita, Y., Iino, M., and Kasai, H. (2001). Dendritic spine geometry is critical for AMPA receptor expression in hippocampal CA1 pyramidal neurons. Nat. Neurosci. *4*, 1086–1092.

Miller, J.C., Silverman, S.K., England, P.M., Dougherty, D.A., and Lester, H.A. (1998). Flash decaging of tyrosine sidechains in an ion channel. Neuron *20*, 619–624.

Minor, D.L., Jr., Masseling, S.J., Jan, Y.N., and Jan, L.Y. (1999). Transmembrane structure of an inwardly rectifying potassium channel. Cell *96*, 879–891.

Mulder, J., Aguado, T., Keimpema, E., Barabás, K., Ballester Rosado, C.J., Nguyen, L., Monory, K., Marsicano, G., Di Marzo, V., Hurd, Y.L., et al. (2008). Endocannabinoid signaling controls pyramidal cell specification and long-range axon patterning. Proc. Natl. Acad. Sci. USA *105*, 8760–8765.

Nadeau, H., McKinney, S., Anderson, D.J., and Lester, H.A. (2000). ROMK1 (Kir1.1) causes apoptosis and chronic silencing of hippocampal neurons. J. Neurophysiol. *84*, 1062–1075.

Nichols, C.G., and Lopatin, A.N. (1997). Inward rectifier potassium channels. Annu. Rev. Physiol. *59*, 171–191.

Okazaki, A., Sudo, Y., and Takagi, S. (2012). Optical silencing of C. elegans cells with arch proton pump. PLoS ONE *7*, e35370.

Parrish, A.R., She, X., Xiang, Z., Coin, I., Shen, Z., Briggs, S.P., Dillin, A., and Wang, L. (2012). Expanding the genetic code of Caenorhabditis elegans using bacterial aminoacyl-tRNA synthetase/tRNA pairs. ACS Chem. Biol. *7*, 1292–1302.

Philipson, K.D., Gallivan, J.P., Brandt, G.S., Dougherty, D.A., and Lester, H.A. (2001). Incorporation of caged cysteine and caged tyrosine into a transmembrane segment of the nicotinic ACh receptor. Am. J. Physiol. Cell Physiol. *281*, C195–C206.

Plaster, N.M., Tawil, R., Tristani-Firouzi, M., Canún, S., Bendahhou, S., Tsunoda, A., Donaldson, M.R., Iannaccone, S.T., Brunt, E., Barohn, R., et al. (2001). Mutations in Kir2.1 cause the developmental and episodic electrical phenotypes of Andersen's syndrome. Cell *105*, 511–519.

Priori, S.G., Pandit, S.V., Rivolta, I., Berenfeld, O., Ronchetti, E., Dhamoon, A., Napolitano, C., Anumonwo, J., di Barletta, M.R., Gudapakkam, S., et al. (2005). A novel form of short QT syndrome (SQT3) is caused by a mutation in the KCNJ2 gene. Circ. Res. *96*, 800–807.

Raimondo, J.V., Kay, L., Ellender, T.J., and Akerman, C.J. (2012). Optogenetic silencing strategies differ in their effects on inhibitory synaptic transmission. Nat. Neurosci. *15*, 1102–1104.

Rhee, H., Lee, J.S., Lee, J., Joo, C., Han, H., and Cho, M. (2008). Photolytic control and infrared probing of amide I mode in the dipeptide backbone-caged with the 4,5-dimethoxy-2-nitrobenzyl group. J. Phys. Chem. B *112*, 2128–2135.

Saito, T. (2006). In vivo electroporation in the embryonic mouse central nervous system. Nat. Protoc. *1*, 1552–1558.

Sandoz, G., Levitz, J., Kramer, R.H., and Isacoff, E.Y. (2012). Optical control of endogenous proteins with a photoswitchable conditional subunit reveals a role for TREK1 in GABA(B) signaling. Neuron *74*, 1005–1014.

Sekar, R.B., Kizana, E., Smith, R.R., Barth, A.S., Zhang, Y., Marbán, E., and Tung, L. (2007). Lentiviral vector-mediated expression of GFP or Kir2.1 alters the electrophysiology of neonatal rat ventricular myocytes without inducing cytotoxicity. Am. J. Physiol. Heart Circ. Physiol. *293*, H2757–H2770.

Shen, B., Xiang, Z., Miller, B., Louie, G., Wang, W., Noel, J.P., Gage, F.H., and Wang, L. (2011). Genetically encoding unnatural amino acids in neural stem cells and optically reporting voltage-sensitive domain changes in differentiated neurons. Stem Cells *29*, 1231–1240.

Szobota, S., and Isacoff, E.Y. (2010). Optical control of neuronal activity. Annu. Rev. Biophys. *39*, 329–348.

Tabata, H., and Nakajima, K. (2001). Efficient in utero gene transfer system to the developing mouse brain using electroporation: visualization of neuronal migration in the developing cortex. Neuroscience *103*, 865–872.

Tao, X., Avalos, J.L., Chen, J., and MacKinnon, R. (2009). Crystal structure of the eukaryotic strong inward-rectifier K+ channel Kir2.2 at 3.1 A resolution. Science *326*, 1668–1674.

Wang, L., and Schultz, P.G. (2004). Expanding the genetic code. Angew. Chem. Int. Ed. Engl. *44*, 34–66.

Wang, L., Brock, A., Herberich, B., and Schultz, P.G. (2001). Expanding the genetic code of Escherichia coli. Science *292*, 498–500.

Wang, L., Xie, J., and Schultz, P.G. (2006). Expanding the genetic code. Annu. Rev. Biophys. Biomol. Struct. *35*, 225–249.

Wang, W., Takimoto, J.K., Louie, G.V., Baiga, T.J., Noel, J.P., Lee, K.F., Slesinger, P.A., and Wang, L. (2007). Genetically encoding unnatural amino acids for cellular and neuronal studies. Nat. Neurosci. *10*, 1063–1072.

Wang, Q., Parrish, A.R., and Wang, L. (2009). Expanding the genetic code for biological studies. Chem. Biol. *16*, 323–336.

Xiao, J., Zhen, X.G., and Yang, J. (2003). Localization of PIP2 activation gate in inward rectifier K+ channels. Nat. Neurosci. *6*, 811–818.

Yizhar, O., Fenno, L.E., Davidson, T.J., Mogri, M., and Deisseroth, K. (2011). Optogenetics in neural systems. Neuron *71*, 9–34.

Yu, C.R., Power, J., Barnea, G., O'Donnell, S., Brown, H.E., Osborne, J., Axel, R., and Gogos, J.A. (2004). Spontaneous neural activity is required for the establishment and maintenance of the olfactory sensory map. Neuron *42*, 553–566.

Zaddam, S., Sacconi, S., Desnuelle, C., Amri, E., and Said, B. (2012). The potassium channel Kir2.1 activity is required for osteoblastogenesis. Biophys. J. *102*, 538a.

Zhang, F., Wang, L.P., Brauner, M., Liewald, J.F., Kay, K., Watzke, N., Wood, P.G., Bamberg, E., Nagel, G., Gottschalk, A., and Deisseroth, K. (2007). Multimodal fast optical interrogation of neural circuitry. Nature *446*, 633–639.